

Beyond the training set: an intuitive method for detecting distribution shift in model-based optimization

Farhan Damani* David H. Brookes* Theodore Sternlieb Cameron Webster
Stephen Malina Rishi Jajoo Kathy Lin Sam Sinai†

Dyno Therapeutics

Abstract

Model-based optimization (MBO) is increasingly applied to design problems in science and engineering. A common scenario involves using a fixed training set to train models, with the goal of designing new samples that outperform those present in the training data. A major challenge in this setting is distribution shift, where the distributions of training and designed samples are different. While some shift is expected, as the goal is to create better designs, this change can negatively affect model accuracy and subsequently, design quality. Despite the widespread nature of this problem, addressing it demands deep domain knowledge and artful application. To tackle this issue, we propose a straightforward method for design practitioners that detects distribution shifts. This method trains a binary classifier using knowledge of the unlabeled design distribution to separate the training data from the design data. The classifier’s logit scores are then used as a proxy measure of distribution shift. We validate our method in a real-world application by running offline MBO and evaluate the effect of distribution shift on design quality. We find that the intensity of the shift in the design distribution varies based on the number of steps taken by the optimization algorithm, and our simple approach can identify these shifts. This enables users to constrain their search to regions where the model’s predictions are reliable, thereby increasing the quality of designs.

1 Introduction

Machine learning (ML) is increasingly used to guide design processes in a variety of disciplines, including materials science, chemistry, and biology [11, 1, 38, 35]. In a typical design problem, one aims to find settings of an input variable that improves an associated property of interest. Such techniques have been used to design, for example, peptide sequences with improved antimicrobial properties [12], or features of superconductors that maximize the critical temperature of superconductivity [8]. Traditional design methods often involve repeated cycles of costly and time-consuming experiments [3]. ML-guided design attempts to reduce the time and cost associated with such design cycles by replacing or augmenting the experimental measurements with predictions produced by an ML model [39].

A popular framework for ML-guided design is offline model-based optimization (MBO) [26, 34]. In this approach, one uses an initial training set of input-property pairs to fit a “surrogate” model that predicts property values from inputs. Then, one searches the space of possible input values to find a new batch of inputs with predicted property values that are greater than those observed in the training set. This search may be carried out by fully or partially optimizing the surrogate model using any number of optimization methods, such as evolutionary algorithms in the case of discrete input spaces, or gradient-based approaches in the case of continuous input spaces.

A major appeal of MBO is its conceptual simplicity. Both the predictive modeling and search steps typically use black-box approaches and thus can be applied to a variety of design problems without expert knowledge in the design domain as long as an initial data set is available. Despite this apparent simplicity, MBO is accompanied by a number of inherent challenges that can render the method ineffective in practice unless great care is taken in its implementation [9]. The most salient of these challenges is that black-box search methods based on optimization will often focus their search on regions of input space that are out-of-distribution (OOD) compared to the initial training data. In other words, there is often a “distribution shift” between the training data and the input regions that are searched. It is well known that many black-box predictive models, such as deep learning models, behave unpredictably when provided OOD inputs, and may produce arbitrarily incorrect predictions in such cases. In the worst case, a search method will exploit pathological predictions in OOD regions (e.g. exceedingly high predictions in a maximization

*These authors contributed equally to this work

†Correspondence: sam.sinai@dynotx.com

problem) to produce inputs that have poor properties in practice, or are even nonsensical [4]; we refer to such inputs as “adversarial examples”.

Detecting distribution shifts from the training data, and identifying the resulting adversarial examples, is the primary challenge in implementing effective MBO techniques. Several methods have been proposed to control the search in MBO such that the design inputs have minimal distribution shift to the initial training data. These methods take various forms, including using Bayesian Optimization techniques to regularize the search with predictive uncertainty of the surrogate model [29], limiting the search to regions with high likelihood in the training distribution [4, 19, 2], or incorporating domain-specific prior information into the search algorithm [27]. While these methods may reduce the likelihood of adversarial examples, they do not entirely mitigate the effects of distribution shift, and are often difficult to tune to the needs of a specific problem.

A different emerging direction in reducing distribution shift is the use of foundation models trained on all known proteins [20, 18], where the set of data in the training domain is expansive. However, while they are the go-to choice for zero-shot generation, design with these models is nascent, and they are not better than supervised approaches when some functional data has already been collected [7].

We propose a simple technique for detecting distribution shifts in MBO. This method not only addresses several of the previously mentioned challenges but can also be combined with any existing design method to further minimize adversarial designs. In particular, we propose training a binary classifier to distinguish between the initial training samples and a separate set of samples drawn from one’s chosen search algorithm. We demonstrate that the logit score output by the trained “OOD classifier” is an interpretable and effective metric for determining which designed sequences are OOD and thus are associated with unreliable predictions from the surrogate model. This method is straightforward to implement given the initial training set and a search method, and can be used in conjunction with any black-box surrogate model and search method. We suggest multiple ways in which the OOD classifier score (henceforth referred to as “OOD scores”) can be used to guide the selection of designed inputs for subsequent experimental verification.

We study the OOD classifier in three increasingly realistic problems. The first is an illustrative toy problem with a two-dimensional input space. Next, we validate the method in a simulated environment for protein structure prediction of a small protein, where we can use *in silico* structure prediction methods to measure the effectiveness of our black-box design. Finally, we apply our method in a real-world experiment where we design Adeno-Associated Virus (AAV) capsid sequences, a complex protein of major importance to gene therapy. We trace the generated sequences over the course of MBO trajectories where they are experimentally tested for multiple important properties. This unique dataset allows us to track the extent and effects of distribution shift during MBO, and test how methods such as the OOD classifier are able to detect such a shift. We show that the OOD classifier can improve the outcome in this black-box design problem, which is inaccessible to structural and domain-informed approaches.

2 Methods

2.1 Offline Model Based Optimization

The objective in a data-driven design problem is to identify an optimal input \mathbf{x}^* of some ground-truth function, $f(\mathbf{x})$, that encodes a scalar property of the input. This can be expressed as the objective $\mathbf{x}^* = \arg \max_{\mathbf{x} \in \mathcal{X}} f(\mathbf{x})$, where \mathcal{X} is a bounded set that we refer to as the “input space” of the problem. The input space may be a discrete or continuous space, and $f(\mathbf{x})$ is typically assumed to be a black box from which we can only make zeroth-order evaluations. We assume the availability of a static dataset, $D = \{(\mathbf{x}_i, y_i)\}_{i=1}^N$, consisting of elements of the input space paired with corresponding noise-corrupted evaluations of the ground truth function.

In MBO, the design strategy is to train a surrogate model $\hat{f}(\mathbf{x})$ on the dataset D using an appropriate supervised regression strategy (e.g. minimizing the mean squared error of predictions from the model via stochastic gradient descent). This surrogate model is then used to guide a search around the input space to find inputs with high predicted property values. This search may take the form of an optimization algorithm [27, 2], probabilistic sampling method [4], or sampling from a generative model [11, 19, 21].

In an ideal scenario for MBO, the inputs of the training dataset would be evenly distributed across the input space, and therefore the error between the surrogate model and the ground truth function would be roughly equal in all regions of input space. In such a case, one could safely optimize the surrogate model directly with a reasonable assumption that this would produce an input that is close to a local optimum of the ground truth function. In most practical scenarios, however, the training inputs are not evenly distributed, and are instead concentrated in a small region of input space. In such cases, the error of the surrogate model will change drastically depending on which region of input space is being tested. Further, search methods that use the

surrogate model will tend to move to regions of input space where there is a low density of training points, and therefore predictions from the surrogate model may be unreliable [4, 9]. In other words, the design strategy induces a distribution shift between the training distribution and the “design distribution” that results from performing the search [10, 37].

In the next section, we discuss the type of distribution shift commonly observed in design problems and how we may be able to detect which inputs are most affected by this shift.

2.2 Distribution shift in design

Covariate shift in regression problems arises when the training data D , sourced from $\mathbf{x}_i \sim p_{\text{tr}}(\mathbf{x})$ and $y_i \sim p(y|\mathbf{x}_i)$, differs from the test input distribution $p_{\text{te}}(\mathbf{x}) \neq p_{\text{tr}}(\mathbf{x})$ [25]. Despite this shift, ground truth labels remain consistently drawn from $p(y|\mathbf{x}_i)$. In the classical covariate shift setting, test sequences are drawn from an independent, distinct distribution.

In MBO, the design algorithm uses predictions under a surrogate model to guide its exploration of input space, which creates a feedback system, leading to querying the model with inputs that can be drastically different from the distribution of inputs observed during training. These inputs all have high predicted scores under the surrogate model, $\hat{f}(\mathbf{x})$. Such test inputs are directly influenced by the training data, leading to a type of distribution shift known as feedback covariate shift (FCS) [10, 31]. Under FCS, the test distribution is given by the design distribution, denote by $p_{\text{de}}(\mathbf{x})$, which differs from a standard test distribution in that it is conditioned on the training set, D . While our method detects various covariate shifts, we emphasize its efficacy against FCS, where predictions can be particularly unreliable.

Figure 1 shows an example of how covariate shift typically manifests itself in MBO. The details of this design problem are presented in Section 4.3; briefly, we optimized a surrogate model using a discrete optimization method to identify protein sequences with high predicted values for a desired property. We included sequences from each point along the optimization trajectory in a bulk physical experiment to (i) determine whether the sequences corresponded to proteins that satisfied basic functional properties, and thus were not adversarial examples, and (ii) evaluate the true property value associated with the sequence. Figure 1a shows that the predictions of the surrogate model increase along the optimization trajectory, as is expected since the surrogate model is the objective function of the optimization. Figure 1b then demonstrates that the error in these surrogate model predictions compared to the ground truth property value increases dramatically along the trajectory, indicating that a covariate shift occurred over the course of the design process. Notably, this dramatic increase in error occurs *despite the surrogate model achieving low MSE on a randomly held out set of data* from the training distribution, as can be seen in the inset of Figure 1b. Finally, Figure 1c shows that at later points in the optimization process, most designs are adversarial sequences that do not satisfy certain basic requirements of a functional protein, further indicating that a severe distribution shift occurred in the design.

Our central aim is to detect when a covariate shift such as that shown in Figure 1 has occurred, so that input points associated with reliable predictions from the surrogate model can be identified. This allows one to avoid selecting inputs for experimental validation that may have unreliable predictions. In order to detect such shifts, we require a score, $s(\mathbf{x})$ that reports the extent, or “intensity” of the shift at each input point. An intuitive score that has been frequently used is the density ratio between the test distribution (in our case, the design distribution) and train distribution [32]:

$$s(\mathbf{x}) = \frac{p_{\text{de}}(\mathbf{x})}{p_{\text{tr}}(\mathbf{x})}. \quad (1)$$

For the purpose of detecting covariate shifts that induce error in the surrogate model, Equation 1 is not necessarily the ideal score. In particular, one should expect $1/p_{\text{tr}}(\mathbf{x})$ to be correlated with the error of the surrogate model at a point \mathbf{x} , but the density of the design distribution should not necessarily impact the surrogate error. However, estimating the density of a high-dimensional distribution such as $p_{\text{tr}}(\mathbf{x})$ can be difficult in practice [13, 36], while we will see that the density ratio $s(\mathbf{x})$ is simple to estimate using a binary classifier. Further we provide a simple argument in Appendix B: to suggest that the $1/p_{\text{tr}}(\mathbf{x})$ term will tend to dominate the difference in scores between two nearby designed inputs; therefore the distinction between $s(\mathbf{x})$ and $1/p_{\text{tr}}(\mathbf{x})$ is small in practice and both can be used to detect distribution shift that results in surrogate model error.

2.3 Distribution shift detection with binary classification

It is well known that a binary classifier can be trained such that its output values approximate a density ratio such as that in Equation 1. In particular, let $g(\mathbf{x})$ be a model with a single continuous scalar output, and let $\rho(\mathbf{x}) = \sigma(g(\mathbf{x}))$ be the probability score of such a model, where σ represents the sigmoid function. Let $p_{\text{de}}(\mathbf{x})$ and $p_{\text{tr}}(\mathbf{x})$ represent the distribution of positive and negative class

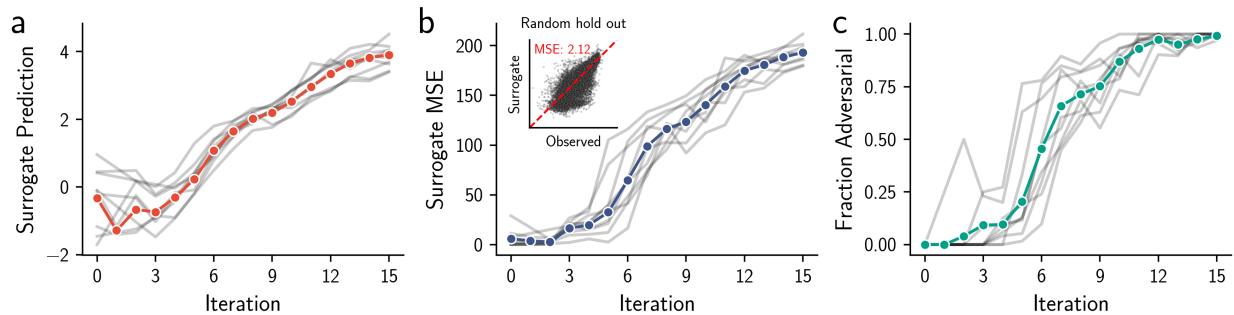


Figure 1: Distribution shift in a protein design problem. Independent trajectories of discrete iterative optimization were run using a surrogate model of a desired property as the objective function and sequences generated along the trajectory were evaluated experimentally. Each subplot shows statistics associated with these trajectories; gray lines correspond to individual trajectories and colored lines display the mean values over all trajectories. (a) Predicted property value from the surrogate model. (b) MSE between surrogate predictions and observed experimental measurement of the property. Inset shows surrogate predictions versus observed property values for a randomly held out set of data from the training distribution. (c) Fraction of sequences observed to be adversarial examples.

inputs, respectively. Then, the binary cross-entropy loss to distinguish between these two classes is:

$$L(\rho) = \mathbb{E}_{p_{\text{tr}}(\mathbf{x})}[-\log(1 - \rho(\mathbf{x}))] + \mathbb{E}_{p_{\text{de}}(\mathbf{x})}[-\log \rho(\mathbf{x})] \quad (2)$$

We follow [30] and take the functional derivative of L with respect to ρ , resulting in

$$\frac{\delta L}{\delta \rho} = \frac{p_{\text{tr}}(\mathbf{x})}{1 - \rho(\mathbf{x})} - \frac{p_{\text{de}}(\mathbf{x})}{\rho(\mathbf{x})} \quad (3)$$

Setting this expression equal to zero demonstrates that the minimizer of the binary cross entropy can be used to exactly predict the OOD score $s(\mathbf{x})$:

$$s(\mathbf{x}) = \frac{p_{\text{de}}(\mathbf{x})}{p_{\text{tr}}(\mathbf{x})} = \frac{\rho(\mathbf{x})}{1 - \rho(\mathbf{x})}. \quad (4)$$

The equivalence shown in Equation 4 is often referred to as the “density ratio trick” and provides a straightforward path towards estimating the OOD scores $s(\mathbf{x})$. In practice, we cannot exactly minimize Equation 2 with respect to ρ , so we parameterize g with parameters θ , and minimize Equation 2 with respect to θ . We then calculate approximate OOD scores as:

$$\hat{s}(\mathbf{x}) = \frac{\rho_{\theta}(\mathbf{x})}{1 - \rho_{\theta}(\mathbf{x})} \quad (5)$$

where $\rho_{\theta}(\mathbf{x}) = \sigma(g_{\theta}(\mathbf{x}))$ are the probability scores associated with the parameterized model $g_{\theta}(\mathbf{x})$. In all of our experiments, g_{θ} is instantiated as either a multi-layer perceptron (MLP) or convolutional neural network (CNN); however, any model architecture could be used within this framework.

2.4 Selection using OOD scores

The final step of any MBO procedure is selecting one or more inputs sampled from the design distribution for follow-up evaluation on the ground truth function (i.e. testing the inputs’ property values in a physical experiment). We propose using the approximate OOD scores calculated via Equation 5 to guide this selection process. Our experiments will demonstrate these OOD scores provide an interpretable metric for detecting distribution shift in MBO methods, and can reliably identify regions of input space where we can expect a surrogate model to make accurate predictions. Given a set of designed inputs, a distribution shift-aware selection procedure should prioritize inputs associated with high surrogate model predictions that are also expected to be accurate based on OOD scores. How exactly a practitioner chooses to enforce this intuition will ultimately be application-specific, and should be tailored to the user’s needs and level of risk-tolerance. Three possible techniques for doing so are (i) a cutoff process, where only allows an input to be selected if $\rho_{\theta}(\mathbf{x}) < c$ for a chosen cutoff value c , (ii) stratified selection in which selects a specified number of inputs from ranges of OOD scores (e.g. select ten inputs from scores between a and b , and 10 inputs from scores between b and c) and (iii) selection based on a user-defined utility function.

2.5 Deploying offline MBO in the wild

The primary aim of creating new offline MBO algorithms is to deploy them in real-world scenarios. However, methods development faces a gap between simulation and the real world. Typically,

methods development is relegated to simulation, and in the rare cases where real-world deployment is involved, the goal is to use the method to produce an optimized design. We are aware of no instances where offline MBO has been applied in real-world situations specifically to study the algorithm itself. Studying offline MBO in real-world settings is essential for improving algorithm development and understanding where simulations break down. The experimental setup for analyzing offline MBO retrospectively can differ in crucial aspects from the usual optimization process aimed at improving a design. Consider the following example. The distribution of designed inputs will gradually shift away from the training data with each optimization step. To study this shift and to determine the limitations of offline MBO, it is crucial to label data at every step to understand where our predictions become inaccurate. On the other hand, if the sole objective is to optimize, there is no need to waste valuable resources on assessing inputs that likely don't improve design. Herein, we design a real-world dataset to study distribution shifts and to evaluate our method in the wild. In the related work section, we discuss the state of datasets in offline MBO and some of its limitations.

3 Related Work

Regularized search in ML-guided design The OOD classifier method is inspired by ML-guided design methods that constrain search to regions close to the training distribution. One approach involves “latent space optimization”, where an encoder-decoder model is trained jointly with a supervised model to map the latent space to property values. After training, optimization is performed in the latent space to find points with high predicted property values, which are then decoded to generate actual designs. This optimization stays close to the training distribution through a spherical boundary constraint [11] or by implicitly modifying the training objective [6]. Another approach focuses on adaptive generative modeling, in which the model parameters are iteratively updated to generate inputs with high predictions based on a surrogate model. To stay close to the training distribution, points can be weighted by their density in the training distribution [4] or by ensuring gradual updates of the weights [12]. Notably, while these approaches require specific surrogate models or search strategies, the OOD classifier can be flexibly paired with any surrogate model or search technique.

[10] proposes an MBO method that adapts conformal prediction methods to FCS. This ensures that search is limited to inputs where the surrogate model can be guaranteed to make accurate predictions. [31] adapts these conformal prediction methods for use within Bayesian Optimization [29]. While these strategies effectively mitigate the effects of FCS, they are computationally intensive and require knowledge of conformal prediction in order to implement. In contrast, the OOD classifier method can be implemented by any practitioner with basic knowledge of ML fundamentals, and our results will indicate that it can also detect FCS.

Density ratio estimation for covariate shift and outlier detection The density ratio between test and train distributions (e.g., Equation 1), has been widely used to address covariate shift in supervised and reinforcement learning. In supervised learning, when the test set is shifted from the training set, the density ratio, $w(\mathbf{x}) := p_{te}(\mathbf{x})/p_{tr}(\mathbf{x})$, can be used to minimize a loss function, $\ell(\mathbf{x}, y)$, averaged over a test set based on the equivalence $\mathbb{E}_{p_{te}(\mathbf{x}, y)}[\ell(\mathbf{x}, y)] = \mathbb{E}_{p_{tr}(\mathbf{x}, y)}[w(\mathbf{x})\ell(\mathbf{x}, y)]$ [25, 32]. This led to techniques for estimating $w(\mathbf{x})$ using binary classifiers and the density ratio trick [33]. In reinforcement learning, the density ratio helps regularize policies in off-policy and off-line RL [24], reweighting marginal state-action pairs during training to avoid low-support regions. However, while these techniques address non-feedback covariate shift, they can not be applied in the feedback case because this requires the surrogate model to already be trained in order to generate the test distribution, $p_{de}(\mathbf{x})$. Thus, we apply the density ratio score in Equation 1 to detect covariate shift of designed inputs instead of weighting samples during training.

Our use of OOD scores at test time is most similar to how density ratio estimates are used to detect outliers in a test set, such as by [13]. Our methods and results differ from this work in a few notable ways. First, we use deep binary classifiers in order to estimate density ratios, in contrast to the linear models used in [13]. Further, the outlier detection task only requires detection of standard (non-feedback) covariate shift; in contrast, our result demonstrates the density ratios can be used to mitigate the effects of feedback covariate shift, and thus can be used for ML-guided design problems. Finally, our results show that OOD scores can be used as a continuous measure that reports on the degree of distribution shift intensity at any point in input space, rather than only for the binary classification task of outlier detection.

Datasets in sequence design While the ML-guided sequence design field has produced a wide variety of datasets and benchmarks in recent years, there remains a gap in understanding how offline MBO methods will perform in the real-world given their performance in these simulated settings.

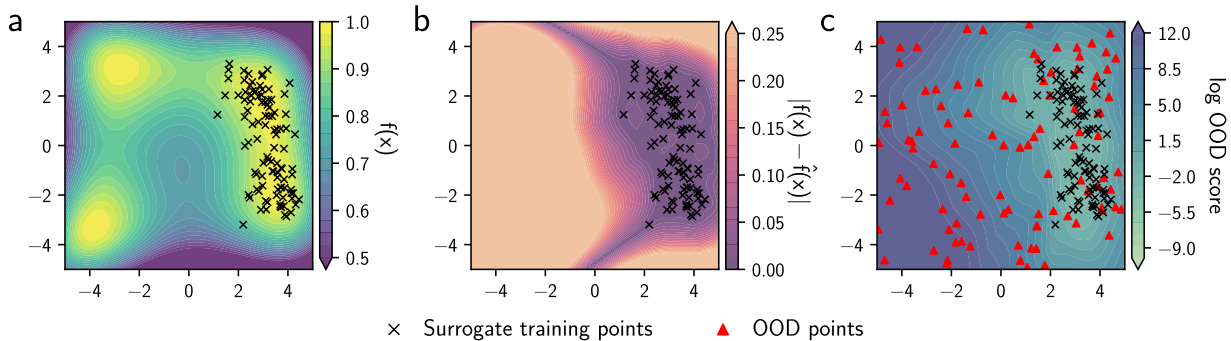


Figure 2: Two-dimensional test of the OOD classifier. (a) The ground truth function, $f(\mathbf{x})$, that we aim to estimate with a surrogate model. Scatter points indicate the training data used to fit the surrogate model. (b) Absolute error between the trained surrogate model $\hat{f}(\mathbf{x})$ and the ground truth function. (c) Logarithm of the OOD scores produced by an OOD classifier that was trained using the black and red scatter points as negative and positive training examples, respectively. Arrows on the ends of colorbars indicate that all values in the direction of the arrow are shown as the same color.

Some examples of progress in dataset development and benchmarking include the following. In protein engineering, one of the more active subdomains where offline MBO has been applied, FLIP [7] curated published data and developed tasks and metrics for model generalization, emphasizing dataset-splitting techniques to probe generalization for offline static datasets. There has also been efforts towards producing comprehensive (i.e., combinatorially complete) low-dimensional datasets [23]. These datasets are useful for evaluating supervised model performance, but are not suitable for evaluating design methods. Outside of protein engineering, Design-Bench [34] consolidates offline MBO challenges across problem domains, allow for algorithm evaluation in a variety of simulated contexts. There exists very few examples of real-world evaluation of design strategies, and none that explicitly study distribution shift [5, 20]. In the next section, we will use a two-dimensional example to illustrate our method and then evaluate its performance in a real-world deployment of offline MBO.

4 Results

4.1 2D Toy model

We first demonstrate the utility of the OOD classifier in a two-dimensional toy problem. The goal here is to learn a surrogate model of a ground truth function, $f(\mathbf{x})$, and to determine the regions in input space where the surrogate model’s predictions are reliable. We employ a modified Himmelblau function [14] as the ground truth. This function is negated and normalized such that all function values are between 0 and 1 in the range $[-5, 5]$ of both input dimensions. The Himmelblau function is commonly used for testing non-convex optimization methods because it contains multiple local optima. We illustrate a case where the training data for the surrogate model is limited to a small region of the input space mimicking real-world problems, such as in protein engineering, where data usually clusters around a natural sequence that represents a local optima. Figure 2a shows the ground truth function along with the positions of the training inputs for the surrogate model. For this example, the training data labels are the exact values of the ground truth function at the input points, with no noise added, i.e. $y_i = f(\mathbf{x}_i)$.

We fit a two-layer MLP to the training data using the MSE loss and the Adam optimizer [16]. Figure 2b shows the absolute error between the surrogate model, $\hat{f}(\mathbf{x})$, and the ground truth function across the input space. As expected, errors increase in regions far from the training data. In a design setting, we might optimize the surrogate model over the input space to find points with increased ground truth values relative to the points in the training set. This optimization can be effective if properly constrained to low-error regions near the training data, but might fail if the optimization can stray to other regions where the model predictions are unreliable. In offline MBO, we are unable to query the ground truth function, which means we need a method to identify trustworthy regions to constrain our search *a priori*. To identify these regions, we trained a (separate) two-layer MLP binary classifier, using the surrogate model’s input training points as negative (in-distribution) training examples and points uniformly sampled across the input space as positive (OOD) examples. We then used Equation 5 to calculate OOD scores for points in the input space; these scores are shown in Figure 2c, along with the positions of the positive and negative training examples. Comparing Figs 2b and 2c, high OOD scores align with areas where surrogate model predictions deviate from the ground truth.

In this toy model, the “design distribution” is the uniform distribution over the input space,

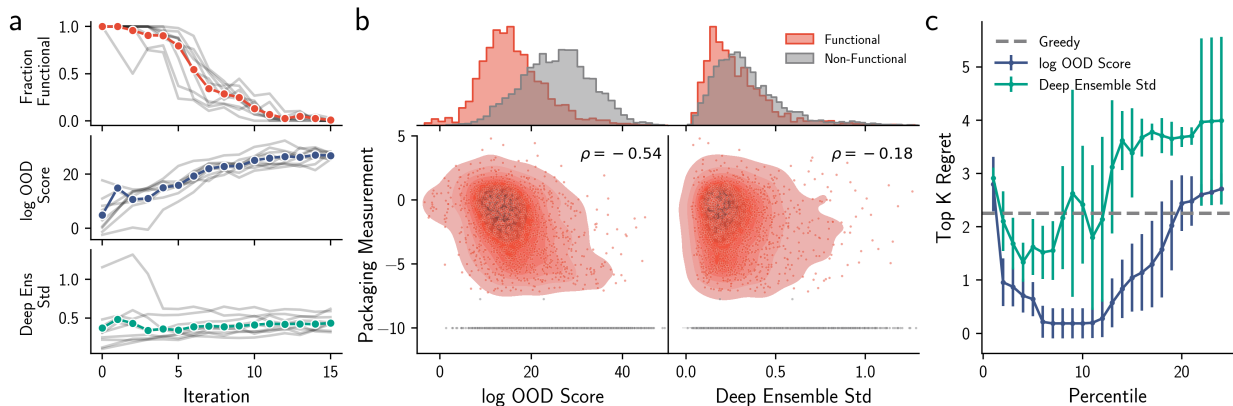


Figure 3: Application of OOD classifier to AAV engineering. (a) Experimental observation and distribution shift detection metrics over the course of design trajectories. x-axis and lines are as in Figure 1; y-axes represent the fraction of functional viruses (top), the logarithm of the OOD scores from the OOD classifier (middle) and the standard deviation of a deep ensemble (bottom) evaluated on each designed sequence. (b) Comparison of distribution shift detection metrics with experimental packaging measurement. Each scatter point represents a sequence; red points indicate functional variants and gray points indicate non-functional variants. Shaded regions are a Kernel Density Estimate (KDE) of the scatter points. Histogram (top) shows distribution of distribution shift metrics for functional and non-functional variants. (c) Evaluation of design selection using distribution shift metrics. Horizontal axis indicates the cutoff percentile of selected distribution shift detection metrics among designed sequences; Vertical axis represents the difference between the maximum observed transduction in the entire dataset and in the set of $K = 100$ sequences with the largest predicted transduction and distribution shift detection metric below the cutoff indicated by the horizontal axis. Error bars represent standard deviation estimates over 50 bootstrap resamples. Grey dashed line represents regret for $K = 100$ sequences selected greedily by predicted transduction without filtering by distribution detection metrics.

making OOD scores proportional to $1/p_{tr}(\mathbf{x})$. This score is a more suitable predictor surrogate model error than $s(\mathbf{x})$, as discussed in Section 2.2. While estimating this ratio is straightforward in a low-dimensional 2D space, it can be exceedingly difficult in high-dimensional spaces where $p_{tr}(\mathbf{x})$ may be arbitrarily complex. Therefore, in most practical cases, we select positive OOD examples from areas likely to be explored by a search method. These are regions of the input space that are unlikely to be densely sampled by a uniform sampling scheme, but are the most important for detecting distribution shift in designed inputs. This more focused strategy results in an OOD classifier that approximates the density ratio $s(\mathbf{x})$.

4.2 Simulated Protein Structure Design

As a sanity check before our real-world experiment, we also develop a proof-of-concept simulation scheme. We rely on protein folding prediction models [15, 18] and devise a task to optimize the folding of a small protein to its target structure, using ESMfold as a ground truth simulator. We see signs of distribution shifts caused by design, and our method can aid in selecting designed inputs by lowering regret (performance of best design vs. the performance of best possible design) when selecting top candidates. However, simulation settings are less relevant when real experiments can be done, and hence we focus the body of the paper on the latter. Interested readers can find the details in Appendix C:.

4.3 Real-world application to the design of AAV capsid protein

We next apply our method to the design of AAV sequences. AAVs are small viruses that have been repurposed as delivery vehicles for gene therapies. Because of the complex processes involved in gene delivery, it is a real-world black box. Previous studies have demonstrated the potential of ML to improve various properties of AAVs such as manufacturability and transduction efficiency (i.e. how well the viruses can deliver genetic material to specific tissues or cell types) [22, 5].

We consider the problem of designing AAV variants that maximize transduction in cell culture. A necessary precursor to successfully delivering genetic material is the proper folding of the viral capsid and encapsulation of the virus’s genetic material, processes that we collectively refer to as “packaging”. We refer to variants that do not package as “non-functional”. Both packaging and transduction can be quantitatively measured experimentally using standard sequencing-based techniques (see Appendix A.2 for details).

Our aim with generating data for this problem was to overcome the issues with testing MBO methods described in Section 2.5 by inspecting mutational trajectories at many points over the

course of a design procedure. We began by following a standard MBO procedure. First, we used an initial training dataset containing AAV sequence variants associated with packaging and transduction measurements to train surrogate models $\hat{f}_{\text{pkg}}(\mathbf{x})$ and $\hat{f}_{\text{tsd}}(\mathbf{x})$ to predict packaging and transduction, respectively, for a given sequence \mathbf{x} . We then used AdaLead, a simple algorithm previously shown to be effective for biological sequence design applications [27], to optimize $\hat{f}_{\text{tsd}}(\mathbf{x})$ under the constraint that $\hat{f}_{\text{pkg}}(\mathbf{x}) > \gamma$ for a chosen cutoff γ . AdaLead maintains a pool of N candidate sequences and iteratively updates this pool in a greedy manner to optimize the objective function. Because genetic algorithms are local search methods, we run the optimization starting from 9 distinct starting sequences for 15 iterations each. To study variability across search methods, we also used a variant of beam search to generate another pool of designed sequences for experimental validation; the details of this method and results associated with these sequences can be found in Appendix A.2. After the design was completed, measured packaging and transduction experimentally for all $15N$ sequences generated along each trajectory, for a total of about 5,000 sequences. Figure 1 shows various properties of this data as a function of algorithm iteration; in particular, this figure demonstrates that a significant distribution shift occurs over the course of the design trajectories. The top panel in Figure 3a additionally shows the fraction of functional viruses generated at each step of the design. Since all designed sequences were predicted to package, the drop in the number of functional sequences demonstrates the frequency of adversarial examples.

We tested two metrics for detecting distribution shift on this data. The first are the OOD scores output by an OOD classifier trained using the initial surrogate models’ training inputs as negative examples, and the designed sequences as positive examples. The second are the standard deviations of predictions from an ensemble of surrogate models, which we refer to as Deep Ensemble uncertainties [17]. The middle and bottom panels of Figure 3a show the values of these metrics as a function of the optimization iteration. We can see that the OOD scores steadily increase over the course of the trajectory, in concert with the increase in surrogate model MSE shown in Figure 1b. This shows that the OOD scores can be effectively used as a continuous predictor of the intensity of distribution shift at points along a design trajectory, rather than only as a binary predictor of whether a point is in- or out-of-distribution. In contrast, the Deep Ensemble scores cannot effectively serve as a quantitative predictor of shift intensity.

Figure 3b compares the distribution shift detection metrics to packaging measurements for all designed sequences. The upper histograms compare the ability of the detection metrics to separate Functional and Non-Functional designed variants. Clearly, the OOD scores are better able to distinguish between these two categories than the Deep Ensemble uncertainties, indicating that the OOD scores can be used to determine whether a designed sequence is adversarial. Further, the lower KDE plots demonstrate that the OOD scores are a fairly reliable predictor of the continuous packaging measurement, again indicating that the OOD scores can be used as a continuous indicator of the intensity of distribution shift at a given input point.

We next evaluate using the OOD scores for selecting designed sequences, as discussed in Section 2.4. Typically, a designer will use surrogate model scores to select a small subset of designed sequences for experimental validation. We replicate this by selecting only K designed sequences out of all designs (for which in this case we know, but don’t use, the ground truth). Using a cutoff scheme, sequences with the highest predicted transduction values were chosen after filtering out sequences with a distribution shift score above a certain threshold (e.g., OOD score > 10). We use regret as our success measure, which measures the gap between the maximum transduction value found in the full set and the K selected sequences. Figure 3c displays this regret across various cutoffs and 50 bootstrap data samples (computed by randomly resampling the full dataset with replacement). We used percentiles for the cutoffs to enable comparison between the OOD score and Deep Ensemble uncertainty. Selecting sequences with OOD scores consistently led to lower regret compared to selecting with Deep Ensemble uncertainty, even achieving zero regret in a number of cases. We note that the regret eventually increases as the cutoff is increased because more adversarial examples are included in the set of selected sequences, replacing the sequences with higher observed transduction. See Appendix A.2 for analogous regret plots at multiple settings of K and for different statistics of the observed transduction values in the selected set.

5 Discussion

We propose a method for addressing distribution shifts that occur during sequence design campaigns. Our approach involves training a binary classifier to distinguish between the training data and the unlabeled designed sequences. We demonstrate that the logit scores outputted by the model serve as a useful scoring function for identifying different levels of distribution shift intensity. Additionally, we discuss the challenges associated with evaluating offline model-based optimization methods using static offline datasets. To overcome this, we run a real-world experiment where we deploy offline MBO in a challenging task for the purpose of algorithm development itself. This

allows us to study the interplay between model-based optimization and distribution shift, rather than solely evaluating whether a design algorithm produced an optimized design. Experimental validation of our method shows that this simple approach can effectively detect distribution shifts and improve established design approaches when used in conjunction.

References

- [1] E. C. Alley, G. Khimulya, S. Biswas, M. AlQuraishi, and G. M. Church. Unified rational protein engineering with sequence-based deep representation learning. *Nature Methods*, 16(12):1315–1322, 2019.
- [2] C. Angermueller, D. Dohan, D. Belanger, R. Deshpande, K. Murphy, and L. Colwell. Model-based reinforcement learning for biological sequence design. In *International conference on learning representations*, 2019.
- [3] F. H. Arnold. Design by directed evolution. *Accounts of Chemical Research*, 31(3):125–131, 1998.
- [4] D. H. Brookes, H. Park, and J. Listgarten. Conditioning by adaptive sampling for robust design. In K. Chaudhuri and R. Salakhutdinov, editors, *Proceedings of the 36th International Conference on Machine Learning*, volume 97 of *Proceedings of Machine Learning Research*, pages 773–782. PMLR, 09–15 Jun 2019.
- [5] D. H. Bryant, A. Bashir, S. Sinai, N. K. Jain, P. J. Ogden, P. F. Riley, G. M. Church, L. J. Colwell, and E. D. Kelsic. Deep diversification of an AAV capsid protein by machine learning. *Nature Biotechnology*, pages 1–6, 2021.
- [6] E. Castro, A. Godavarthi, J. Rubinfien, K. Givechian, D. Bhaskar, and S. Krishnaswamy. Transformer-based protein generation with regularized latent space optimization. *Nature Machine Intelligence*, 4(10):840–851, 2022.
- [7] C. Dallago, J. Mou, K. E. Johnston, B. Wittmann, N. Bhattacharya, S. Goldman, A. Madani, and K. K. Yang. FLIP: Benchmark tasks in fitness landscape inference for proteins. In *Thirty-fifth Conference on Neural Information Processing Systems Datasets and Benchmarks Track (Round 2)*, 2021.
- [8] C. Fannjiang and J. Listgarten. Autofocused oracles for model-based design. In H. Larochelle, M. Ranzato, R. Hadsell, M. F. Balcan, and H. Lin, editors, *Advances in Neural Information Processing Systems*, volume 33, pages 12945–12956. Curran Associates, Inc., 2020.
- [9] C. Fannjiang and J. Listgarten. Is novelty predictable? *arXiv preprint arXiv:2306.00872*, 2023.
- [10] C. Fannjiang, S. Bates, A. N. Angelopoulos, J. Listgarten, and M. I. Jordan. Conformal prediction under feedback covariate shift for biomolecular design. *Proceedings of the National Academy of Sciences*, 119(43):e2204569119, 2022.
- [11] R. Gómez-Bombarelli, J. N. Wei, D. Duvenaud, J. M. Hernández-Lobato, B. Sánchez-Lengeling, D. Sheberla, J. Aguilera-Iparraguirre, T. D. Hirzel, R. P. Adams, and A. Aspuru-Guzik. Automatic Chemical Design Using a Data-Driven Continuous Representation of Molecules. *ACS Central Science*, 4(2):268–276, 2018.
- [12] A. Gupta and J. Zou. Feedback GAN for DNA optimizes protein functions. *Nature Machine Intelligence*, 1(2):105–111, 2019.
- [13] S. Hido, Y. Tsuboi, H. Kashima, M. Sugiyama, and T. Kanamori. Statistical outlier detection using direct density ratio estimation. *Knowledge and Information Systems*, 26(2):309–336, 2011.
- [14] D. M. Himmelblau. *Applied Nonlinear Programming*. McGraw-Hill, 1972.
- [15] J. Jumper, R. Evans, A. Pritzel, T. Green, M. Figurnov, O. Ronneberger, K. Tunyasuvunakool, R. Bates, A. Žídek, A. Potapenko, A. Bridgland, C. Meyer, S. A. A. Kohl, A. J. Ballard, A. Cowie, B. Romera-Paredes, S. Nikolov, R. Jain, J. Adler, T. Back, S. Petersen, D. Reiman, E. Clancy, M. Zielinski, M. Steinegger, M. Pacholska, T. Berghammer, S. Bodenstein, D. Silver, O. Vinyals, A. W. Senior, K. Kavukcuoglu, P. Kohli, and D. Hassabis. Highly accurate protein structure prediction with AlphaFold. *Nature*, 596(7873):583–589, 2021.

- [16] D. Kingma and J. Ba. Adam: A method for stochastic optimization. In *International Conference on Learning Representations (ICLR)*, San Diego, CA, USA, 2015.
- [17] B. Lakshminarayanan, A. Pritzel, and C. Blundell. Simple and Scalable Predictive Uncertainty Estimation using Deep Ensembles. In I. Guyon, U. V. Luxburg, S. Bengio, H. Wallach, R. Fergus, S. Vishwanathan, and R. Garnett, editors, *Advances in Neural Information Processing Systems*, volume 30. Curran Associates, Inc., 2017.
- [18] Z. Lin, H. Akin, R. Rao, B. Hie, Z. Zhu, W. Lu, N. Smetanin, R. Verkuil, O. Kabeli, Y. Shmueli, A. dos Santos Costa, M. Fazel-Zarandi, T. Sercu, S. Candido, and A. Rives. Evolutionary-scale prediction of atomic-level protein structure with a language model. *Science*, 379(6637):1123–1130, 2023.
- [19] J. Linder, N. Bogard, A. B. Rosenberg, and G. Seelig. A Generative Neural Network for Maximizing Fitness and Diversity of Synthetic DNA and Protein Sequences. *Cell Systems*, 11(1):49–62.e16, 2020.
- [20] A. Madani, B. Krause, E. R. Greene, S. Subramanian, B. P. Mohr, J. M. Holton, J. L. Olmos Jr, C. Xiong, Z. Z. Sun, R. Socher, et al. Large language models generate functional protein sequences across diverse families. *Nature Biotechnology*, pages 1–8, 2023.
- [21] E. Nijkamp, J. Ruffolo, E. N. Weinstein, N. Naik, and A. Madani. Progen2: exploring the boundaries of protein language models. *arXiv preprint arXiv:2206.13517*, 2022.
- [22] P. J. Ogden, E. D. Kelsic, S. Sinai, and G. M. Church. Comprehensive AAV capsid fitness landscape reveals a viral gene and enables machine-guided design. *Science*, 366(6469):1139–1143, 2019.
- [23] F. J. Poelwijk, M. Socolich, and R. Ranganathan. Learning the pattern of epistasis linking genotype and phenotype in a protein. *Nature Communications*, 10(1):4213, 2019.
- [24] D. Precup, R. S. Sutton, and S. P. Singh. Eligibility traces for off-policy policy evaluation. In *Proceedings of the Seventeenth International Conference on Machine Learning, ICML '00*, page 759–766, San Francisco, CA, USA, 2000. Morgan Kaufmann Publishers Inc.
- [25] H. Shimodaira. Improving predictive inference under covariate shift by weighting the log-likelihood function. *Journal of Statistical Planning and Inference*, 90(2):227–244, 2000.
- [26] S. Sinai and E. D. Kelsic. A primer on model-guided exploration of fitness landscapes for biological sequence design. *arXiv:2010.10614*, 2020.
- [27] S. Sinai, R. Wang, A. Whatley, S. Slocum, E. Locane, and E. D. Kelsic. Adalead: A simple and robust adaptive greedy search algorithm for sequence design, 2020.
- [28] M. Smith. In vitro mutagenesis. *Annual Review of Genetics*, 19(1):423–462, 1985.
- [29] J. Snoek, H. Larochelle, and R. P. Adams. Practical Bayesian Optimization of Machine Learning Algorithms. In F. Pereira, C. J. Burges, L. Bottou, and K. Q. Weinberger, editors, *Advances in Neural Information Processing Systems*, volume 25. Curran Associates, Inc., 2012.
- [30] A. Srivastava, S. Han, K. Xu, B. Rhodes, and M. U. Gutmann. Estimating the density ratio between distributions with high discrepancy using multinomial logistic regression. *Transactions on Machine Learning Research*, 2023.
- [31] S. Stanton, W. Maddox, and A. G. Wilson. Bayesian optimization with conformal prediction sets. In F. Ruiz, J. Dy, and J.-W. van de Meent, editors, *Proceedings of The 26th International Conference on Artificial Intelligence and Statistics*, volume 206 of *Proceedings of Machine Learning Research*, pages 959–986. PMLR, 25–27 Apr 2023.
- [32] M. Sugiyama, S. Nakajima, H. Kashima, P. Buenau, and M. Kawanabe. Direct Importance Estimation with Model Selection and Its Application to Covariate Shift Adaptation. In J. Platt, D. Koller, Y. Singer, and S. Roweis, editors, *Advances in Neural Information Processing Systems*, volume 20. Curran Associates, Inc., 2007.
- [33] M. Sugiyama, T. Suzuki, and T. Kanamori. *Density Ratio Estimation in Machine Learning*. Cambridge University Press, 2012.
- [34] B. Trabucco, X. Geng, A. Kumar, and S. Levine. Design-bench: Benchmarks for data-driven offline model-based optimization. In *International Conference on Machine Learning*, pages 21658–21676. PMLR, 2022.

- [35] H. Wang, T. Fu, Y. Du, W. Gao, K. Huang, Z. Liu, P. Chandak, S. Liu, P. Van Katwyk, A. Deac, et al. Scientific discovery in the age of artificial intelligence. *Nature*, 620(7972):47–60, 2023.
- [36] E. Weinstein, A. Amin, J. Frazer, and D. Marks. Non-identifiability and the blessings of misspecification in models of molecular fitness. *Advances in Neural Information Processing Systems*, 35:5484–5497, 2022.
- [37] L. B. Wheelock, S. Malina, J. Gerold, and S. Sinai. Forecasting labels under distribution-shift for machine-guided sequence design. In *Machine Learning in Computational Biology*, pages 166–180. PMLR, 2022.
- [38] Z. Wu, S. J. Kan, R. D. Lewis, B. J. Wittmann, and F. H. Arnold. Machine learning-assisted directed protein evolution with combinatorial libraries. *Proceedings of the National Academy of Sciences*, 116(18):8852–8858, 2019.
- [39] K. K. Yang, Z. Wu, and F. H. Arnold. Machine-learning-guided directed evolution for protein engineering. *Nature methods*, 16(8):687–694, 2019.
- [40] R. Zhou. Trp-cage: Folding free energy landscape in explicit water. *Proceedings of the National Academy of Sciences*, 100(23):13280–13285, 2003.

Appendix A: Experiment details

A.1 2D toy example details

Here we provide more details on the two dimensional toy example discussed in Section 4.1.

Ground truth function The ground truth function in this problem is given by

$$f(\mathbf{x}) = -\frac{1}{m}\text{himm}(\mathbf{x}) + 1 \quad (6)$$

where $m = \max_{\mathbf{x} \in \mathcal{X}} \text{himm}(\mathbf{x})$, with $\mathcal{X} = [-5, 5] \times [-5, 5]$, and $\text{himm}(\mathbf{x})$ is the Himmelblau function, given by

$$\text{himm}(\mathbf{x}) = (x_0^2 + x_1 - 11)^2 + (x_0 + x_1^2 - 7)^2. \quad (7)$$

The modifications to the Himmelblau function in Equation 6 have the dual purpose of (i) negating the function so that the local optima are maxima, which is aligned with the formulation of MBO in Section 2.2 as a maximization problem and (ii) normalizing the function so that all ground truth values are between 0 and 1 in the input space, which enables stable model training.

Training data for surrogate model The training data for the surrogate model was generated by randomly selecting points in the input space according to the distribution

$$p(\mathbf{x}) \propto \begin{cases} \exp(25 \cdot f(\mathbf{x})) & \text{if } x_0 > 0 \\ 0 & \text{otherwise.} \end{cases} \quad (8)$$

Specifically, we created a grid with width 0.005 in each direction over the input space, evaluated each point according to $p(\mathbf{x})$, normalized the probabilities, and sampled 100 points from the grid according to the probabilities. This distribution has the effect of concentrating the training data around the local maxima of the ground truth function in the region $x_0 > 0$. The labels for the sampled training points are simply noiseless evaluations of the ground truth function at those points.

Surrogate model details The surrogate model for this example was an MLP with two fully connected hidden layers with 200 nodes each and ReLU activation functions applied to each hidden layer. The output of the model was scaled using a one-dimensional Batch Normalization. The model was trained by minimizing an MSE loss over 1000 epochs using the Adam algorithm a batch size of 32, an initial learning rate of 1e-3, and a dropout rate of 0.1 for hidden layer parameters.

OOD classifier details The training data for the OOD classifier consisted of (i) the input training points for the surrogate model, associated with a label of 0 representing the “in-distribution” class, and (ii) 100 input points sampled uniformly at random from the input space associated with a label of 1 representing the OOD class. The architecture of the OOD classifier was identical to that of the surrogate model; the only change being the removal of the final batch normalization layer and the addition of L2 regularization over the weights with regularization strength 1e-3, to prevent overfitting. The model was trained by minimizing the binary cross-entropy loss over 1000 epochs using Adam algorithm a batch size of 32, and an initial learning rate of 1e-3, and a dropout rate of 0.1 for hidden layer parameters.

A.2 AAV experiment details

Data generation Both the initial training data and designed data contain AAV variants associated with transduction and packaging measurements. In both datasets, the sequences are variants of the AAV9 wild-type sequence, modified in a 63 amino-acid region containing the VR-IV loop of the VP3 capsid protein. The distribution of edit distances to AAV9 WT for the training and design datasets are shown in Figure 4.

Sequences in the training and designed data were assayed for packaging and transduction using a standard sequencing-based technique [22]. This technique involves first constructing a “library” of plasmid sequences that encode the protein variants of interest. This plasmid library is then subjected to experimental conditions that enable the plasmids to be converted to proteins and assemble into viral capsids, to produce a sample of viruses containing genetic material. This virus sample is then introduced to cells, allowing the viruses to enter these cells and transfer their genetic material to the cell’s nucleus if they are capable of doing so; this is the process known as transduction. The genetic material that successfully entered the nucleus of cells is then collected. At each stage of the experiment, a small sample of genetic material is sequenced using Next Generation Sequencing methods, allowing one to approximate the abundance of each sequence variant in the

plasmid library, the virus sample, and the sample of successfully transduced genetic material. These abundance measurements are in the form of sequencing counts, i.e. the number of times a specific variant appears in the sequencing data. Let n_i^{plasmid} , n_i^{virus} and n_i^{tsd} be the sequencing counts of the i^{th} variant in the plasmid, viral and transduced samples. The ability of variant i to package is then quantified as the log rate:

$$y_i^{\text{pkg}} = \log \frac{n_i^{\text{virus}}}{n_i^{\text{plasmid}}} \quad (9)$$

Similarly, the transduction ability of variant i is quantified as

$$y_i^{\text{tsd}} = \log \frac{n_i^{\text{tsd}}}{n_i^{\text{virus}}}. \quad (10)$$

Design strategy We run offline MBO given a fixed training dataset of $(\mathbf{x}_i, y_i^{\text{pkg}}, y_i^{\text{tsd}})$ triplets, where \mathbf{x}_i is the sequence of variant i . The input space for the design is the space of all amino acid sequences of length 63. Details of the surrogate models and search method used in this MBO design are discussed in turn below.

Surrogate models We trained two surrogate models: $\hat{f}_{\text{pkg}}(\mathbf{x})$ to predict packaging from sequence and $\hat{f}_{\text{tsd}}(\mathbf{x})$ to predict transduction. These packaging and transduction surrogate models were trained using the input-label pairs $(\mathbf{x}_i, y_i^{\text{pkg}})$ and $(\mathbf{x}_i, y_i^{\text{tsd}})$, respectively. Both models had a Convolutional Neural Network (CNN) architecture with following hyperparameters:

- Number of Convolutional Blocks: 2
- Number of Channels: [32, 32]
- Pooling Scales: [0, 0]
- Number of dense layers: 1
- Dense layer size: 32
- activation type: LeakyReLU

Both models were trained by minimizing an MSE loss using the Adam optimization algorithm until convergence using early stopping on a random-holdout validation set (10% of samples) with a patience set to 10 epochs.

Search algorithm We applied two search methods to this problem. The first is AdaLead [27], a variant of a genetic algorithm that has been shown to work well for biological sequence design applications. We refer readers to [27] for a detailed treatment of the AdaLead algorithm. The second search method we applied is a stochastic variant of beam search, with a beam width of 5, maximum number of iterations equal to 15 and a total budget of 5,000.

Results Results for sequences designed with AdaLead are shown in Figure 1 and 3 in the main text. Analogous results for the sequences designed with beam search are shown in Figures 5 and 6, below. We also report additional results for the selection regret experiment shown in Figures 3c and 6. In particular, we show the regret as we vary the number of selected sequences ($K = 10, 50, 100, 250$) and the batch statistic for the selected sequences (90th percentile, 95th percentile, and Max). We show this for the AdaLead design in Figure 7 and the beam search design in Figure 8.

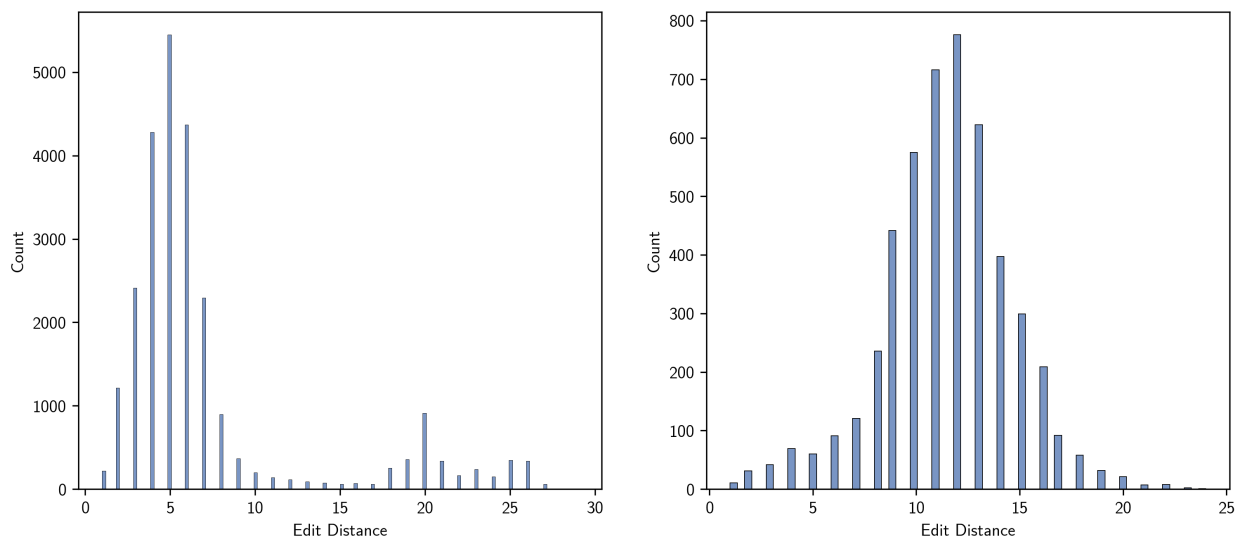


Figure 4: Distribution of edit distances to wild-type for training data (left) and designed data (right).

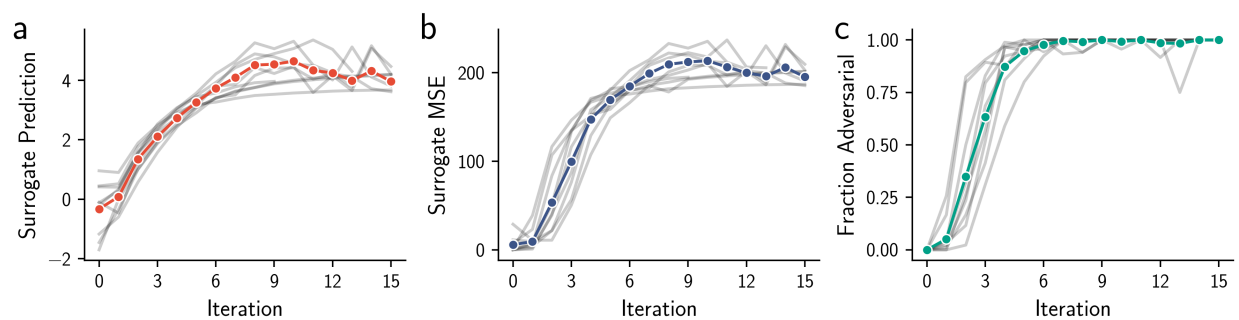


Figure 5: Analysis of distribution shift in AAV variants designed by MBO with beam search as the search method. Plot descriptions are as in Figure 1 in the main text.

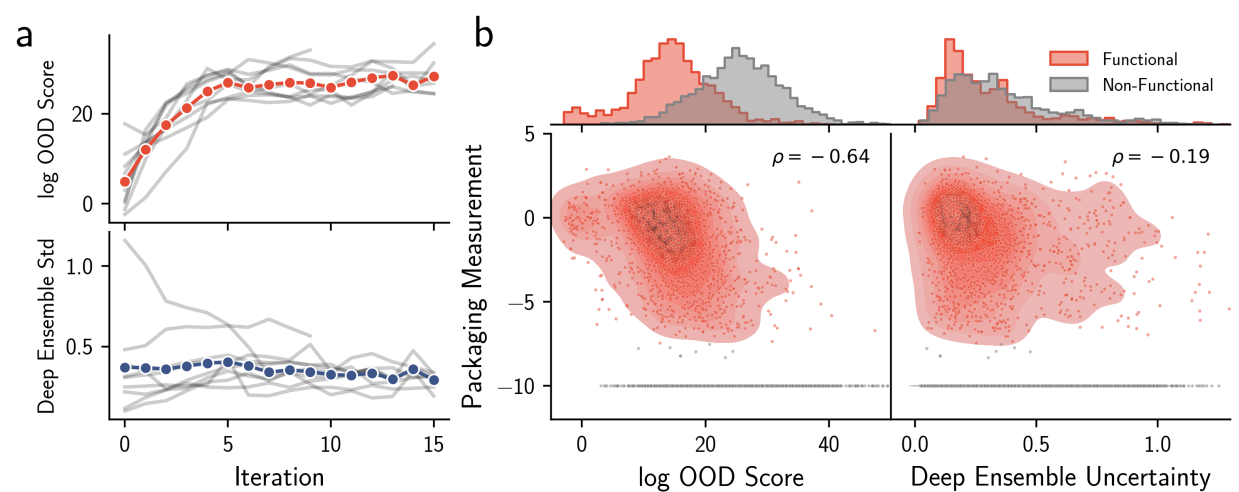


Figure 6: Results applying distribution shift detection metrics to AAV variants designed by MBO with beam search as the search method. Plot descriptions are as in Figure 3 in the main text.

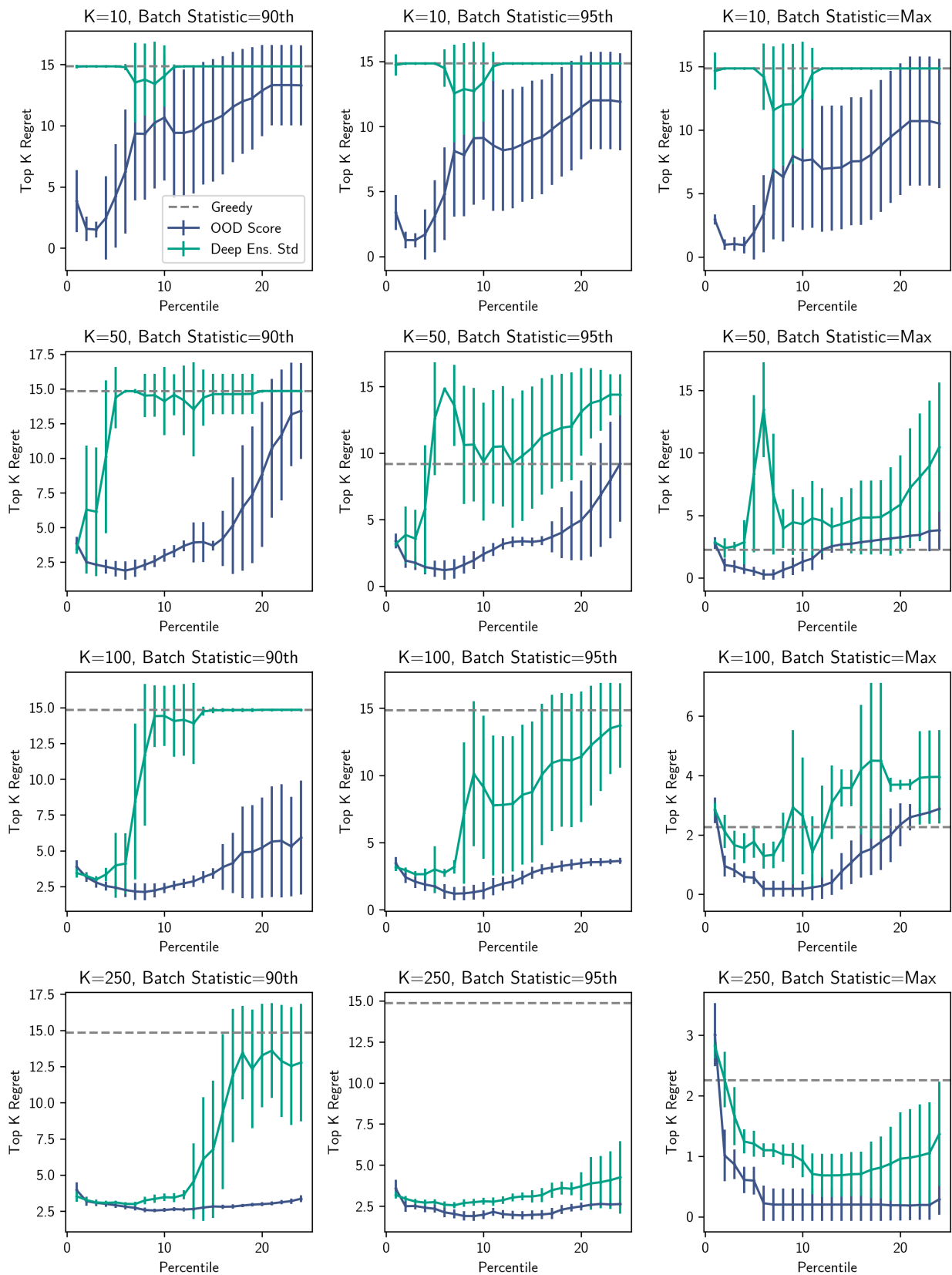


Figure 7: Expanded results of selection regret experiments for AAV variants designed by MBO with AdaLead as the search method. Regret is shown for varying batch sizes (Top K) and batch statistics (90th, 95th, Max). Plot descriptions are as in Figure 3c.

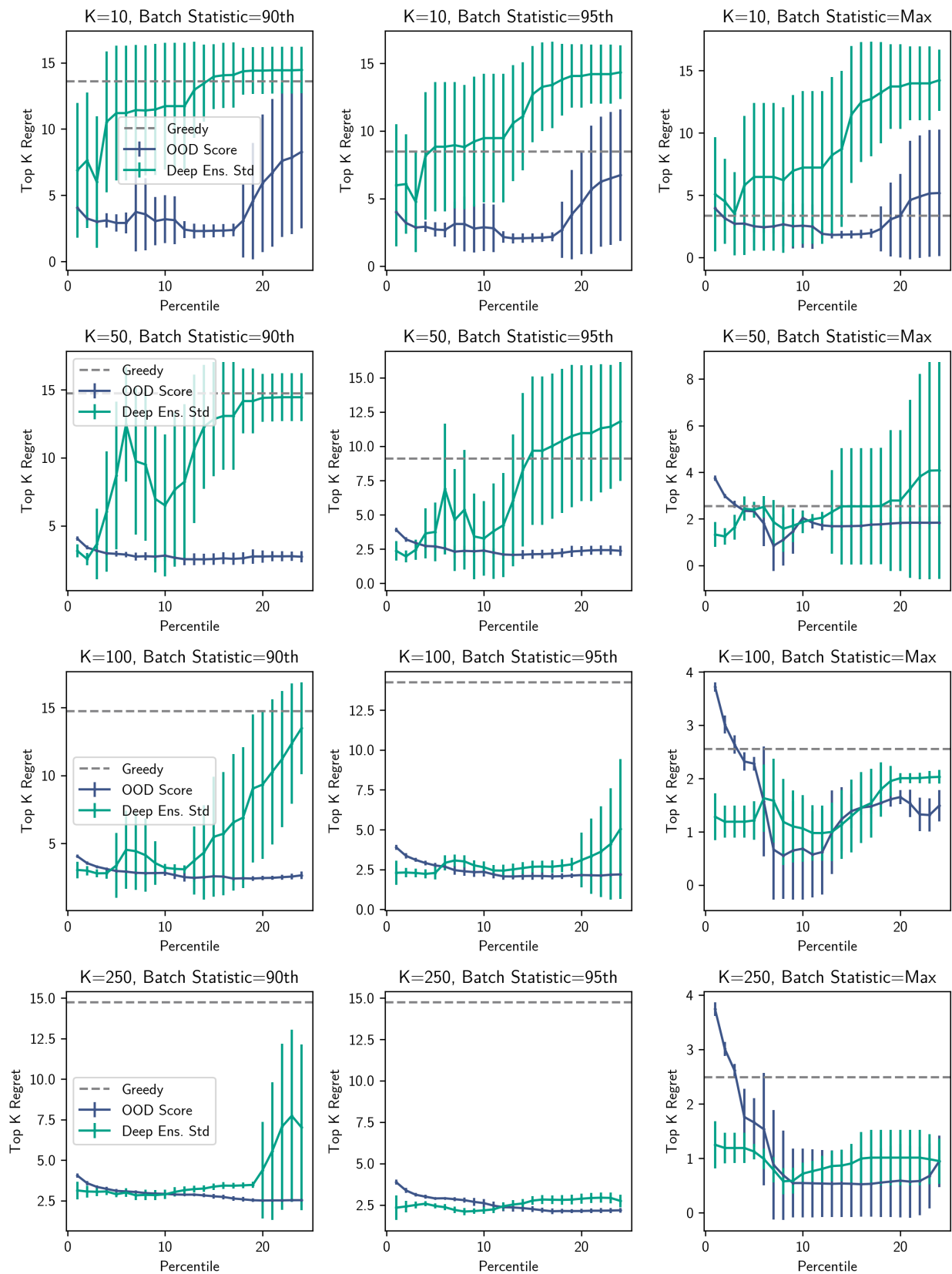


Figure 8: Results of selection regret experiments for AAV variants designed by MBO with beam search as the search method. Regret is shown for varying batch sizes (Top K) and batch statistics (90th, 95th, Max). Plot descriptions are as in Figure 3c

Appendix B: Balance of terms in OOD scores

In Section 2.2, we discuss the distinction between the OOD score, $s(\mathbf{x}) = p_{\text{de}}(\mathbf{x})/p_{\text{tr}}(\mathbf{x})$, and another potential distribution shift detection metric, $1/p_{\text{tr}}(\mathbf{x})$. We suggest that the latter may be a more suitable score for detecting distribution shift that would result in surrogate model error, but use the OOD score instead because it is straightforward to calculate via the density ratio trick. Further, we claim that the difference in OOD scores between two nearby design points will tend to be dominated by the denominator terms in the OOD scores, and thus the distinction between $s(\mathbf{x})$ and $1/p_{\text{tr}}(\mathbf{x})$ will often be negligible in practice. Here, we provide justification for this latter claim by considering a simple one dimensional example. In particular, consider an input point x drawn from a one dimensional design distribution with continuous support, $p_{\text{de}}(x)$, and a nearby point $x + \delta x$. The difference between the log OOD scores of these two points can be approximated by Taylor expanding to first-order:

$$\log s(x + \delta x) - \log s(x) \approx \delta x \frac{d}{dx} \log s(x), \quad (11)$$

which can then be simplified by computing

$$\frac{d}{dx} \log s(x) = \frac{p'_{\text{de}}(x)}{p_{\text{de}}(x)} - \frac{p'_{\text{tr}}(x)}{p_{\text{tr}}(x)}, \quad (12)$$

where prime indicates differentiation with respect to x . Now we assume that both the design and training distribution are Gaussian distributions, with means μ_{de} and μ_{tr} , respectively, and variances σ_{de}^2 and σ_{tr}^2 , respectively. In this case, the difference between the scores is approximately

$$\log s(x + \delta x) - \log s(x) \approx \frac{x - \mu_{\text{tr}}}{\sigma_{\text{tr}}^2} - \frac{x - \mu_{\text{de}}}{\sigma_{\text{de}}^2} \quad (13)$$

We now consider cases where the first term in Equation 13, which corresponds to the $1/p_{\text{tr}}(\mathbf{x})$ term in the OOD score, will be larger than the second term. If the variances of the train and design distributions are roughly similar, then the first term will tend to be larger because x is drawn from the design distribution and is therefore likely to be closer to the mean of the design than the training distribution, as long as these means are well-separated. The impact of the second term will be further reduced if the variance of the design distribution is large compared to that of the train distribution. To summarize, the two conditions that will cause the $1/p_{\text{tr}}(\mathbf{x})$ term to dominate the difference in OOD scores between two nearby points are (1) the means of train and design distribution are well separated and (2) the variance of the design distribution is larger than that of the train distribution.

In practice, both of these conditions are typically satisfied by design distributions. The first condition is satisfied because the design method will tend to search around regions of input space far from the training data (thus inducing the distribution shift that is the focus of this paper). Similarly, the second condition is usually satisfied because the design method will tend to search large regions of the input space to find candidate solutions, producing a large variance in the design distribution. Thus, we can usually assume that the difference in $1/p_{\text{tr}}(\mathbf{x})$ terms is the dominant effect when considering the difference in OOD scores between two input points.

Appendix C: Protein Structure Prediction Experiment

Problem Description Real-world sequence design problems are characterized by high-dimensional discrete input spaces, label noise, and limited training data. While evaluating design methods with physical experiments in the sciences and engineering is the best way to evaluate offline MBO, these experiments can be resource and time-intensive. Therefore, it is valuable to have simulation settings that mimic key aspects of the target problem in order to develop and evaluate methods rapidly [34]. Here we describe a simulation using protein structure prediction [15] as a benchmark for evaluating offline MBO. The challenge in protein structure prediction is to determine the 3D shape of a protein based solely on its amino acid sequence. Knowing this 3D shape is key to understanding how the protein functions and interacts on a molecular level. Deep learning has recently brought about significant advances to the field. AlphaFold2 [15] has achieved impressive accuracy in predicting protein shapes, with some predictions reaching the accuracy levels of experimental methods.

Our proposal is to use a protein structure prediction network as the ground truth function given its broad generalization capabilities across a wide variety of proteins. Concretely, this means our task is to design an amino acid sequence that folds into the ground truth structure for a predefined protein. The ground truth structure is a publicly available experimentally derived structure (e.g., by using X-ray crystallography). Because there are many amino acid sequences that can fold into the same structure, this is a design task to search in the amino acid sequence space for a sequence

that has a predicted structure with the minimum structural distance to the target structure. The wild-type sequence that encodes this structure is intentionally hidden from the model.

Using a protein structure prediction network as a simulated fitness landscape offers several benefits. These networks provide accurate results across various protein types and sequence lengths. They are computationally efficient to query, free from label noise, and allow us to examine performance differences across multiple datasets. Most importantly, we observe distribution shift induced by design, which we find is a salient feature of real-world protein engineering settings.

Our aim is to design a protein sequence that folds into the structure of Trp-Cage [40], a notably compact 20-residue mini protein known for its stable folding and structural elements. To determine how closely the predicted structure of our designed sequence matches the true structure of Trp-Cage, we employ the frame-aligned point error (FAPE) metric [15]. Lower FAPE scores indicate a closer alignment between the predicted and the actual structure of Trp-Cage.

Experimental Design We design a training dataset by employing an in-silico variant of error-prone PCR [28], a lab method that randomly mutates a system by decreasing the precision of DNA replication. Here, we introduce mutations at each position in the wild-type (WT) protein sequence (i.e., an example protein sequence that is known to fold into the target protein structure), based on a specific error rate ϵ . We loop over every position in a sequence and with probability ϵ we mutate each position using a uniform distribution over the 20 canonical amino acids. This process is repeated 10K times to generate a set of unlabeled sequences. In our setting we set ϵ to 0.5, so roughly half of the positions of the wild-type sequence are mutated. This makes the problem sufficiently challenging with a lot of diversity in the sequences (and subsequently the distances between their predicted structures and the ground truth). For each sequence, we compute predicted structures using ESMFold [18] and FAPE scores by comparing each predicted structure to the WT’s known crystal structure. Negative FAPE scores are used as the labels for our dataset since our aim is to minimize the structural distance to the target protein (or maximize the negative FAPE score).

We implement offline MBO with this training dataset. We first fit a surrogate regression model $f(\mathbf{x})$ to the (\mathbf{x}_i, y) pairs, predicting FAPE scores from the amino acid sequence. Then, we design 10K sequences using the same genetic algorithm used in the AAV experiment [27] to maximize $f(\mathbf{x})$. Because genetic algorithms are local search methods, we run the optimization from 10 different starting points corresponding to 10 distinct initial sequences, restart each optimization run with two random initializations, and save designed sequences from iterations 5, 20, 50 corresponding to low, medium, and high shift intensities. After running optimization, we train the OOD classifier to separate the training data (class 0) from the designed data (class 1). We then label our data by using our ground truth function (ESMFold) to compute FAPE scores, measuring the structural distance between each amino acid sequence and our target protein structure.

Design hyperparameters We use an identical set of hyperparameters to what is described in Appendix A.2 for the AAV experiment for the surrogate regression model. For search, we use Adalead [27] as our optimization algorithm with a population size of 1K. We refer readers to [27] on algorithm implementation and recommended hyperparameters.

Results We first show evidence that our simulation shows a distribution shift between the design data and the training data (Fig. 9a and in a more extensive ablation in Fig. 10). Here we evaluate the regression model accuracy (as measured by Spearman Rank Correlation) across optimization steps (holding edit distance fixed to 10) and across edit distances (holding optimization steps fixed at 20). We observe substantial distribution shifts in both settings corresponding to feedback and non-feedback covariate shift.

Next, we show how a distribution shift metric can enable better selection of variants. We follow an identical setup to the AAV experiment described in Section 4.3 and show top K regret for a variety of values of K and batch statistics (90th, 95th, Max) (Fig. 11). In all cases we see the OOD score achieves lower regret than Deep Ensemble Uncertainty.

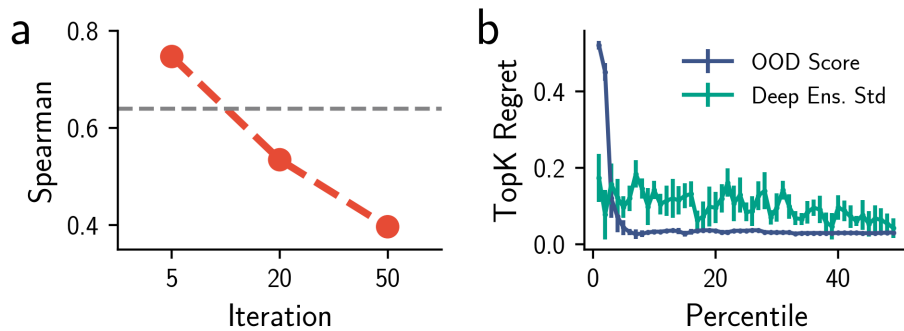


Figure 9: Application of OOD classifier to a protein folding simulation task using a protein structure prediction network as the ground truth oracle. The goal is to design a sequence that folds into a target 3D protein structure. Offline MBO is run on a synthetically generated dataset. (a) Model accuracy along an optimization trajectory. (b) Evaluation of design selection using distribution shift detection metrics.

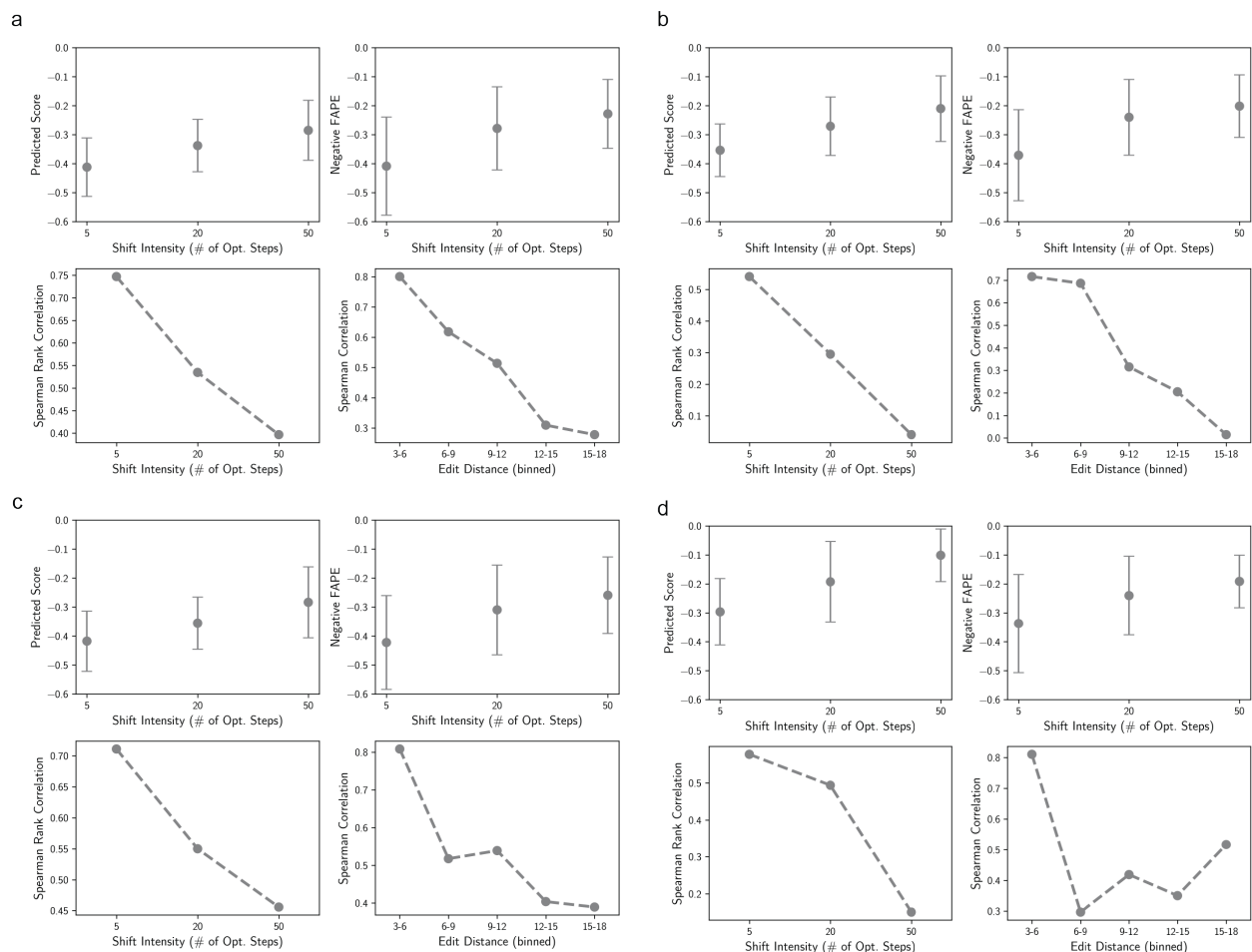


Figure 10: (Top) Predicted score (left) and ground truth measurement (right) increase as a function of optimization step. (Bottom) Model performance decays as a function of optimization step (left) and edit distance (right). Subpanels correspond to four randomly sampled datasets given the parameters to the in-silico error-prone PCR generation procedure.

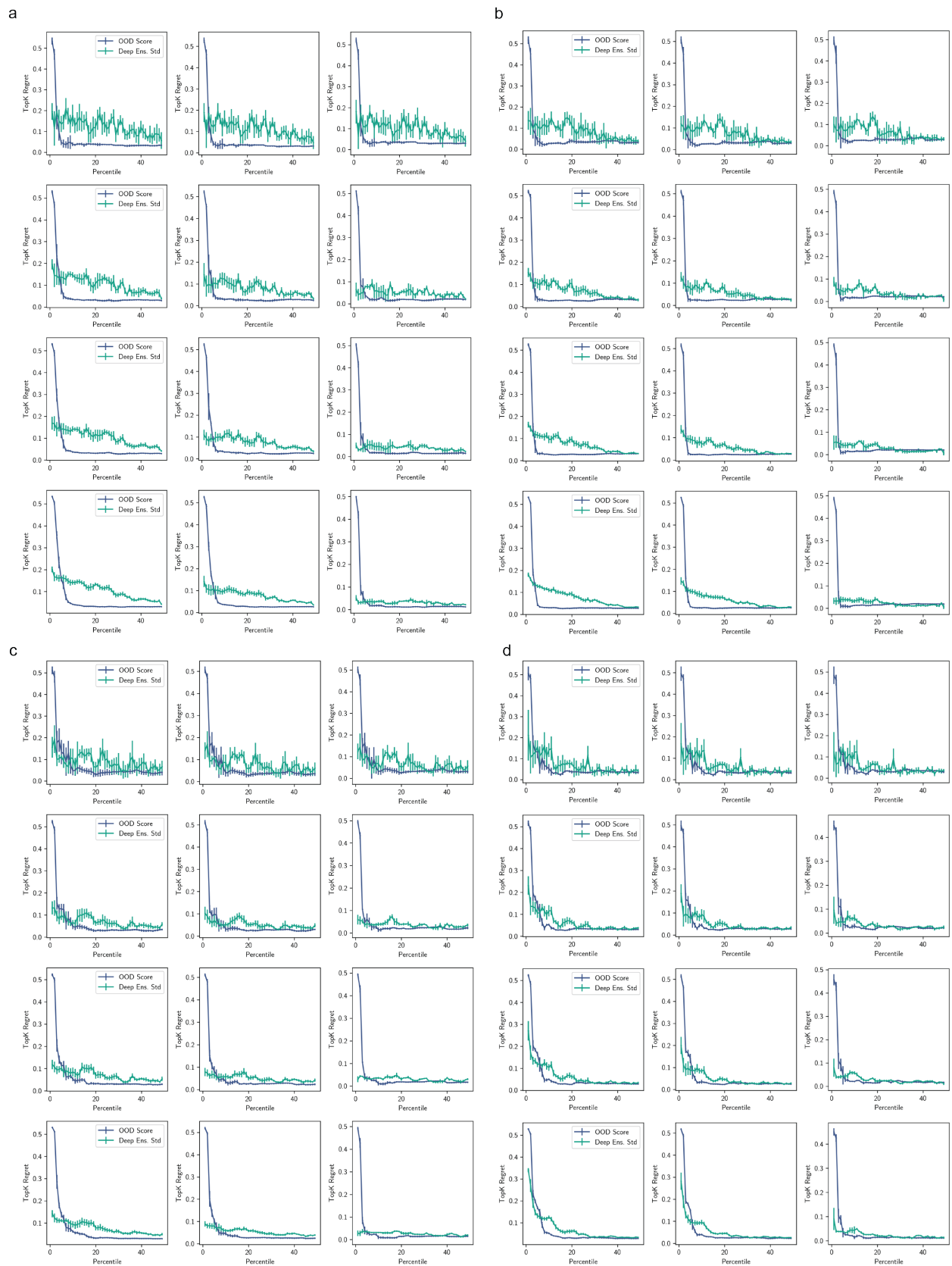


Figure 11: Regret plots for the protein structure prediction task for varying batch sizes and batch statistics. Rows are Top K = 10, 50, 100, 250 and columns are transduction percentiles 90th, 95th, Max. Subpanels correspond to four randomly sampled datasets given the parameters to the in-silico error-prone PCR generation procedure.